JOURNAL OF SOLID STATE CHEMISTRY 92, 273–285 (1991)

Synthesis, Crystal Structure, and Magnetic Properties of $Co_3(HPO_4)_2(OH)_2$ Related to the Mineral Lazulite

J. L. PIZARRO, G. VILLENEUVE, AND P. HAGENMULLER

Laboratoire de Chimie du Solide du CNRS, Université de Bordeaux I, 351, Cours de la Libération, 33405 Talence Cedex, France

AND A. LE BAIL

Laboratoire des Fluorures, URA CNRS 449, Faculté des Sciences, Université du Maine, 72017 Le Mans Cedex, France

Received September 13, 1990; in revised form January 4, 1991

$Co_3(HPO_4)_2(OH)_2$ has a monoclinic symmetry (space group $P2_1/n$), with $a = 7.532(1)$Å, $b = 7.516(1)$Å, $c = 7.700(2)$Å, $\beta = 121.91(1)°$, $Z = 2$. Systematic twinning prevents structural determination from single crystal data. The structure is determined from X-ray powder data by direct methods, the refinements using the Rietveld method ($R_B = 0.043$, $R_{WP} = 0.098$). The hydrogen atoms are located from neutron powder diffraction data. The material is isostructural with the mineral lazulite. Magnetic properties show a rather complex behavior. A metamagnetic transition is observed at $H_c = 0.12$ T below the long range ordering temperature ($T_N = 10.6$ K) The thermal evolution of the magnetic properties above this temperature may be explained by antiferromagnetic coupling between weakly ferromagnetic ordered layers.

Introduction

The magnetostructural properties of vivianite $Fe_3(PO_4)_2 \cdot 8H_2O$ and ludlamite $Fe_3(PO_4)_2 \cdot 4H_2O$ have been intensively studied by susceptibility measurements, Mössbauer spectroscopy, specific heat determinations, and neutron diffraction (*1–7*). It appears that the magnetic behavior of vivianite is rather complex, involving at least two magnetic sublattices which, moreover, are not independent from each other. The magnetic behavior of ludlamite seems to be better understood, the structure consisting of ferromagnetic trimers formed by edge-sharing Fe^{2+} octahedra coupled by an antiferromagnetic intertrimer interaction.

Substitution of Fe^{2+} by Co^{2+} was expected to bring about some modifications of this magnetic behavior, due to the large magnetic anisotropy of Co^{2+} in an octahedral environment. Hence the cobalt analogue of the mineral vivianite has been synthesized and its antiferromagnetic features analyzed (*8*). Using hydrothermal conditions, obtaining the cobalt phosphate tetrahydrate related to ludlamite might have been expected (*1, 9*). Depending on the experimental conditions many phases were actually prepared, but up to now all attempts to

0022-4596/91 $3.00

obtain a cobalt ludlamite have failed. Among the various phases, one of them, $Co_3(HPO_4)_2(OH)_2$, has been identified as related to the mineral lazulite (*10*), $(Mg,Fe)Al_2(PO_4)_2(OH)_2$.

In this article we report the structural characterization and the magnetic properties of $Co_3(HPO_4)_2(OH)_2$.

Experimental

$Co_3(HPO_4)_2(OH)_2$ was prepared from the cobalt phosphate octahydrate $Co_3(PO_4)_2 \cdot 8H_2O$ isostructural with the mineral vivianite $Fe_3(PO_4)_2 \cdot 8H_2O$ (*11, 12*) using hydrothermal conditions. The octahydrate was previously prepared from an aqueous solution of cobalt sulfate and ammonium phosphate at 70°C. The hydrothermal synthesis was carried out in sealed gold tubes at 250°C and 400 atm for 3 days, resulting in apparently well-shaped crystals (typically $0.3 \times 0.5 \times 0.8$ mm^3).

A preliminary XRD powder study did not allow the identification of any of the known phosphate hydrates $Co_3(PO_4)_2 \cdot nH_2O$ (*1*).

A thermogravimetric analysis, carried out with a SETARAM microbalance, under argon atmosphere at 75°C/hr shows a continuous weight loss between 338 and 414°C. The final compound was identified as $Co_3(PO_4)_2$ by its powder X-ray diffraction pattern. The observed weight loss (8.89%) was in good agreement with that expected for two water molecules (8.94%), so that at this stage the formula was believed to be $Co_3(PO_4)_2 \cdot 2H_2O$.

In fact, the absence of any bending band at about 1650 cm^{-1} on the IR vibration spectrum (recorded using a Perkin–Elmer 1430 spectrometer) was inconsistent with the presence of water. A rather sharp band observed at 3530 cm^{-1} emphasizes the presence of $(OH)^-$ groups. Furthermore, bands in the 2850- to 2950-cm^{-1} range and a broad one occuring at 2400–2500 cm^{-1} result from strong bonds involving these $(OH)^-$ groups (*13*). No detailed assignment attempt was made for the bands occuring below 1300 cm^{-1}; they correspond to different P–O modes.

A preliminary X-ray single crystal diffraction study showed evidence of systematic twinning. In spite of numerous attempts, a real single crystal could not be isolated and no solution for a mathematical correction of the twinning effects was found; the symmetry was estimated to be low, probably monoclinic. Such a finding led us to try an ab initio structural determination from powder diffraction data.

The X-ray powder pattern was recorded on a Siemens D501 diffractometer (Cu$K\alpha$, graphite monochromator in the reflected beam). A strong preferred orientation effect was noticed when the sample was packed and a series of harmonics was used for self-calibration (estimation of the zero point before indexing). The pattern used for structure determination was obtained from a sample dusted on its holder through a 63-μm sieve.

In order to localize the hydrogen atoms, a neutron powder diffraction experiment was achieved at 50 K (well above the magnetic ordering temperature). The pattern was recorded on the D1A instrument at Laue Langevin Institute, ILL, Grenoble, the wavelength being 1.909 Å.

The magnetic properties were investigated with a SQUID SHE magnetometer in the temperature range 1.9–250 K. The magnetic susceptibility was measured at $H = 0.1$ T. The magnetization was determined from 0 to 5 T between 1.9 and 25 K.

Crystal Structure

X-Ray Investigation at Room Temperature

Indexing was realized by using the TREOR program (*14*) applied to the first 24 lines of the X-ray pattern. The most probable solution corresponded to a monoclinic

TABLE I

DETAILS OF RIETVELD REFINEMENTS FOR $Co_3(HPO_4)_2(OH)_2$ (SPACE GROUP $P2_1/n$, $Z = 2$)

	X-ray (293 K)	Neutrons (50 K)
Cell parameters		
a(Å)	7.531(1)	7.5024(2)
b(Å)	7.516(1)	7.4896(2)
c(Å)	7.700(2)	7.6716(2)
β(°)	121.91(1)	121.864(1)
Volume(Å^3)	370.0(2)	366.11(4)
Wavelength	Cu$K\alpha$	1.909 Å
2θ range (°)	10–130	0–156
Step scan (°2θ)	0.02	0.05
Number of reflections	625[a]	405
Number of parameters		
Structural	30	34
Total	42	48
Reliability factors		
R_B	0.043	0.035
R_p	0.077	0.018
R_{WP}	0.098	0.021
R_E	0.025	0.022
Background	Subtracted	Not subtracted

[a] Reflections (1 0 −1), (11 -1), (011), (110) at low angle excluded for their high asymmetry

symmetry and was characterized by figures of merit $M_{20} = 28$ and $F_{20} = 37$ (0.011, 50) as defined in Refs. (*15*) and (*16*). The refined cell parameters are given in Table I. The limiting conditions for reflection lead to space group $P2_1/n$.

In order to obtain the maximum number of estimated individual intensities, the profile fitting procedure with cell constraints described in (*17*) was applied. Conventional Rietveld profile reliability factors $R_P = 0.059$ and $R_{WP} = 0.075$ (calculated after background subtraction) for 625 reflections were obtained (*18, 19*). This data set was reduced to 361 $|F_{obs}|$ (reflections closer than 0.04°2θ being excluded). Application of the direct methods (option EEES of the SHELX76 program (20)) provided the starting positions of the cobalt, phosphorus, and three independent oxygen atom sites; the two remaining oxygen atom sites were located thanks to a Fourier difference map. The best residual obtained from this data set was $R = 0.23$ with SHELX76 in the isotropic approximation of thermal motion (the scattering factors and anomalous terms for Co^{2+} and P were taken from the "International Tables for X-Ray Crystallography" (*21*) and for O^{2-} from (*22*)). We then turned back to the Rietveld method. For the last refinement four highly asymmetric low angle reflections were excluded, leading to the final R factors $R_B = 0.043$ and $R_{WP} = 0.098$. The observed and calculated patterns are shown in Fig. 1.

At this stage it was clear that the crystal structure was related to that of the mineral lazulite $(Mg,Fe)Al_2(PO_4)_2(OH)_2$ (*10, 23*). This fact could suggest the presence of both Co^{2+} and Co^{3+} in this material, within the hypothesis of an identical chemical formula. However, UV–visible spectroscopy as well as magnetic behavior (see below) are quite inconsistent with the coexistence of trivalent and divalent cobalt ions. Bond valence calculations according to Brown (*24*) showed a significant deficit of charge for one oxygen atom belonging to the (PO_4) group leading to the probable formulation $Co_3(HPO_4)_2(OH)_2$ with only Co^{2+}. To our knowledge this material is the first monohydrogenphosphate which adopts the lazulite-type structure.

Neutron Diffraction at 50 K

Starting from the coordinates established using X-ray diffraction, the Rietveld profile refinement of the neutron pattern (using the DBW3.2S program (*25, 26*) with a pseudo-Voigt profile-shape function) converged down to $R_B = 0.24$. Then hydrogen atoms were located by Fourier difference synthesis and the final reliability factor dropped to 0.035. Details of the refinement are given in Table I, the final atomic parameters and isotropic B factors in Table II, and selected bond lengths and angles in Table III. Figure 2 shows the observed and calculated neutron pattern of $Co_3(HPO_4)_2(OH)_2$. Due to the large hydrogen content, the background

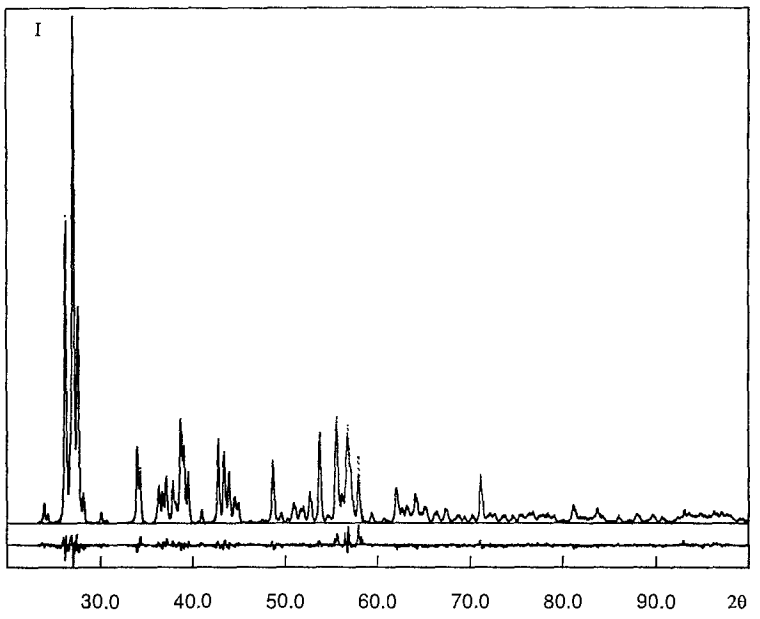

FIG. 1. Observed (···) and calculated (—) X-ray patterns of $Co_3(HPO_4)_2(OH)_2$. Difference function below.

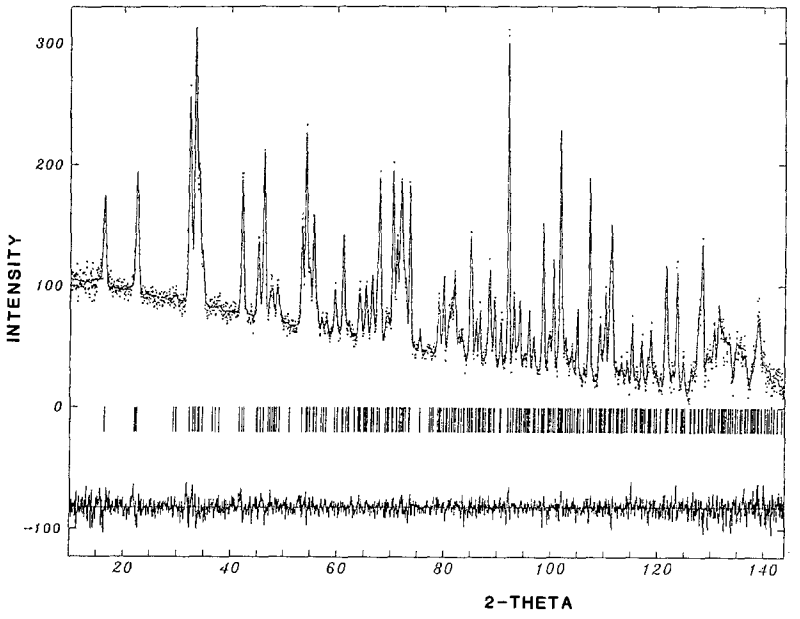

FIG. 2. Observed (···) and calculated (—) neutron patterns of $Co_3(HPO_4)_2(OH)_2$. Difference function below.

TABLE II

ATOMIC COORDINATES AND THERMAL PARAMETERS FOR $Co_3(HPO_4)_2(OH)_2$ FROM NEUTRON DATA (50 K) AND X-RAY DATA (*) (293 K); THE ATOMIC COORDINATES OF $CoSO_4 \cdot H_2O$ (*27*) ARE GIVEN FOR COMPARISON (*Italics*) (e.s.d IN PARENTHESES)

Atom	x	y	z	B(Å^2)
Co(1)	0.223(1)	0.273(1)	0.979(1)	−0.2(1)
*	0.2244(2)	0.2734(2)	0.9806(2)	0.79(3)
Co	*1/4*	*1/4*	*0*	
Co(2)	1/2	0	0	−0.2(1)
*	1/2	0	0	0.17(4)
P	0.9978(9)	0.1172(5)	0.2642(9)	0.18(8)
*	0.9973(4)	0.1170(3)	0.2635(4)	0.85(4)
S	*0*	*0.093*	*1/4*	
O(1)	0.2132(6)	0.0282(5)	0.3867(7)	0.22(4)
*	0.2177(7)	0.0293(7)	0.3896(7)	1.1(1)
O(1)	*0.203*	*−0.017*	*0.362*	
O(2)	0.6758(5)	0.4856(5)	0.3591(6)	0.22(4)
*	0.6728(8)	0.4862(7)	0.3538(8)	2.5(1)
O(1)	*0.703*	*0.483*	*0.362*	
O(3)	0.0181(6)	0.2480(6)	0.1079(6)	0.22(4)
*	0.0153(7)	0.2486(8)	0.1063(7)	2.0(1)
O(2)	*0.021*	*0.196*	*0.104*	
O(4)	0.5497(5)	0.7351(6)	0.1049(7)	0.22(4)
*	0.5432(7)	0.7317(8)	0.0997(7)	1.8(1)
O(2)	*0.521*	*0.696*	*0.104*	
O(5)	0.0312(6)	0.6304(5)	0.2738(7)	0.22(4)
*	0.0260(7)	0.6281(6)	0.2745(7)	0.5(1)
H_2O	*0*	*0.615*	*1/4*	
H(1)	−0.108(1)	0.3273(8)	0.027(1)	1.2(1)
H(2)	0.105(1)	0.5558(9)	0.234(1)	1.2(1)

is high and, in spite of 1-day measurements, the pattern is rather noisy.

Description of the Structure

The lazulite structure has been extensively described in Ref. (*10*) and in a subsequent paper (*23*) presenting a more accurate refinement. To summarize, the crystal structure of $Co_3(HPO_4)_2(OH)_2$ consists of chains of corner-sharing Co(1) octahedra running along the [101] direction, the common corner being the hydroxyl group O(5)H(2). Two parallel chains are linked by Co(2) octahedra, giving rise to Co(1)–Co(2)–Co(1) face-sharing trimers (Fig. 3). Cobalt layers are formed, interconnected by (HPO_4) groups. The main difference be-

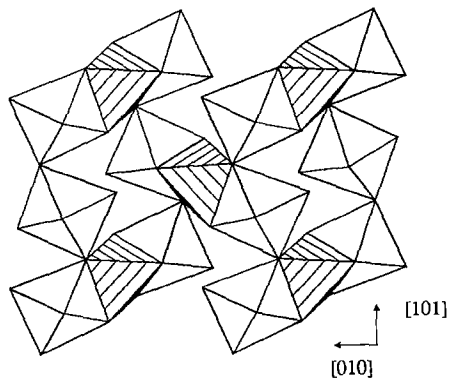

FIG. 3. View of the cobalt octahedra linkage. Chains of the corner sharing Co(1) octahedra (unshaded) are directed toward [101]. Co(2) octahedra (shaded) share faces with two Co(1) octahedra.

TABLE III

SELECTED INTERATOMIC DISTANCES (Å) AND ANGLES (°) FROM THE NEUTRON COORDINATES (50 K) (e.s.d. IN PARENTHESES)

Co(1) octahedron ⟨Co–O⟩ = 2.110

Co(1)	O(5)	O(2)	O(1)	O(5)	O(4)	O(3)
O(5)	2.004(7)	2.976(5)	2.905(5)	4.099(3)	3.225(5)	2.898(7)
O(2)	93.2(5)	2.093(8)	4.194(4)	2.642(5)	2.690(5)	3.239(3)
O(1)	90.0(5)	170.8(4)	2.103(8)	3.200(5)	3.219(3)	2.895(6)
O(5)	170.7(4)	77.9(6)	98.9(4)	2.108(7)	2.667(8)	3.129(6)
O(4)	102.9(4)	79.4(5)	99.4(4)	78.3(6)	2.12(1)	4.334(3)
O(3)	86.2(5)	96.9(4)	83.7(5)	92.2(4)	170.3(3)	2.23(1)

Co(2) octahedron ⟨Co–O⟩ = 2.096

Co(2)	O(2)	O(2)	O(4)	O(4)	O(5)	O(5)
O(2)	2.079(3)	4.157(5)	2.690(5)	3.196(4)	3.249(4)	2.642(5)
O(2)	180.0(3)	2.079(3)	3.196(4)	2.690(5)	2.642(5)	3.249(4)
O(4)	80.2(4)	99.8(3)	2.099(5)	4.198(6)	3.255(4)	2.667(8)
O(4)	99.8(3)	80.2(4)	180.0(3)	2.099(5)	2.667(8)	3.255(4)
O(5)	101.8(3)	78.2(4)	101.3(3)	78.7(5)	2.109(6)	4.218(3)
O(5)	78.2(4)	101.8(3)	78.7(5)	101.3(3)	180.0(2)	2.109(6)

P tetrahedron ⟨P–O⟩ = 1.541

P	O(2)	O(4)	O(1)	O(3)
O(2)	1.504(6)	2.498(3)	2.523(4)	2.536(6)
O(4)	111.7(4)	1.514(9)	2.536(7)	2.511(5)
O(1)	112.6(5)	112.9(5)	1.528(6)	2.474(3)
O(3)	108.7(5)	106.6(5)	103.7(5)	1.617(8)

The hydrogen bonds

O–H···O	O–H	H···O	O–H···O	O–O
O(3)–H(1)···O(1)	1.007(7)	1.614(7)	170.6(9)	2.612(4)
···O(1)		2.02(1)	149.4(7)	2.876(4)
O(5)–H(2)	0.94(1)			
···O(3)		2.452(8)	127.3(6)	3.115(6)
O(1)···H(2)···O(3) 80.0(5)				

Cobalt bridging angles and intercationic distances

(1) Corner sharing Co(1)–Co(1) chains			
Co(1)–O(5)–Co(1)	128.4(4)	Co(1)–Co(1)	3.703(9)
(2) Face sharing Co(1)–Co(2)–Co(1) trimers			
Co(1)–O(2)–Co(1)	86.5(5)	Co(1)–Co(2)	2.859(7)
Co(1)–O(4)–Co(1)	85.4(4)		
Co(1)–O(5)–Co(1)	85.3(5)		
(3) Corner sharing Co(1)–Co(2)			
Co(1)–O(5)–Co(2)	120.1(4)	Co(1)–Co(1)	3.564(4)

tween our phase and lazulite is expected to result from the monohydrogenphosphate group and from a lower electrostatic repulsion inside the trimers due to the 2+ oxidation state of cobalt. In fact both phases show similar rather large distortion of the octahe-

TABLE IV

THE BOND VALENCE CALCULATION COMPUTED ACCORDING TO BROWN (*24*)

Atom	O(1)	O(2)	O(3)	O(4)	O(5)	Σ
Co(1)	0.33	0.34	0.24	0.32	0.33	
					0.44	2.00
Co(2)	—	0.35	—	0.33	0.33	1.01 (×2)
P	1.29	1.38	1.01	1.34	—	5.02
Σ	1.62	2.07	1.25	1.99	1.10	
H(1)	0.26	—	0.73	—	—	0.99
H(2)	0.16	—	0.10	—	0.84	1.10
Σ	2.04	2.07	2.08	1.99	1.94	

dra which are elongated along the cation–cation axis. For instance, the configuration around the Co(2) atom can be described as an almost regular trigonal antiprism, whose bases correspond to the faces shared with neighboring Co(1) octahedra. The six unshared edges are elongated: they range from 3.196 to 3.255 Å (d_{ave} = 3.233 Å) while the shared edges range from 2.642 to 2.690 Å (d_{ave} = 2.666 Å).

A bond valence calculation computed according to Brown (*24*) is given in Table IV. It shows good agreement between the values of the effective charges on the Co, P, and O atoms, except for the oxygen atoms O(1), O(3), and O(5), which exhibit a charge deficit. The lazulite structure has a bifurcated hydrogen bond with two different hydrogen–oxygen distances (*23*):

$$\text{O(5)–H(2)} \begin{matrix} \cdots\text{O(1)}\ 2.26(3)\ \text{Å} \\ \cdots\text{O(3)}\ 2.49(3)\ \text{Å} \end{matrix}$$

$$\text{O(1)}\cdots\text{H(2)}\cdots\text{O(3)}\ 66.8°.$$

An additional hydrogen bond in $Co_3(HPO_4)_2(OH)_2$, P–O(3)–H(1)···O(1) (d = 1.614(7) Å), conerns the same oxygen atom O(1) involved in the similar O(5)–H(2) ···O(1) connection. The bifurcated hydrogen bond is in fact maintained with

$$\text{O(5)–H(2)} \begin{matrix} \cdots\text{O(1)}\ 2.01(1)\ \text{Å} \\ \cdots\text{O(3)}\ 2.452(8)\ \text{Å} \end{matrix}$$

$$\text{O(1)}\cdots\text{H(2)}\cdots\text{O(3)}\ 80.0(5)°.$$

The bond valence calculation computed according to Brown (*24*) is now fully satisfying (Table IV).

A simple relation (which, to our knowledge, had not been so far pointed out) occurs between the lazulite-type structure and the structure adopted by the well known series $M^{II}SO_4 \cdot H_2O$ (M^{II} = Mn, Fe, Co, Ni, Zn, Mg) (*27, 28*) (e.g., $CoSO_4 \cdot H_2O$, space group $C2/c$, a = 6.963 Å, b = 7.580 Å, c = 7.470 Å, β = 116°21, Z = 4) or also by a phosphate $MnPO_4 \cdot H_2O$ (*29*) (Fig. 4). The nonstandard $P2_1/n$ space group was chosen to illustrate this relation (see Table II). One just needs to remove the Co(2) atom; this means that the symmetry of the lazulite-type is pseudo-C-centered, so that the 0,1/2,0 site is almost equivalent to the 1/2,0,0 site for the Co(2) atom. This phenomenon may lead to stacking faults and account thus for easy twinning of the crystals.

Magnetic Properties

The magnetization vs applied field variation obtained at 1.9 K up to 5 T is given in Fig. 5. It increases linearly with the field up to H = 0.12 T, then a sudden enhancement occurs and the magnetization increases again linearly between 2 and 5 T. This phenomenon looks like a metamagnetic behavior for H_c = 0.12 T, but the saturation is not achieved at a field as high as 5 T. Increasing the temperature, the metamagnetic transition is still observed, but it becomes less and less sharp above 10.6 K and it disappears above 18 K (Fig. 6).

The thermal evolution of the magnetic susceptibility has been studied at fields lower than 0.12 T, i.e., in the domain below the metamagnetic transition, when the magnetization varied linearly with the field. A very complex behavior occurs. The thermal variations of χ, χ^{-1}, and χT are shown in Figs. 7, 8, and 9 in order to display clearly all the observed singularities.

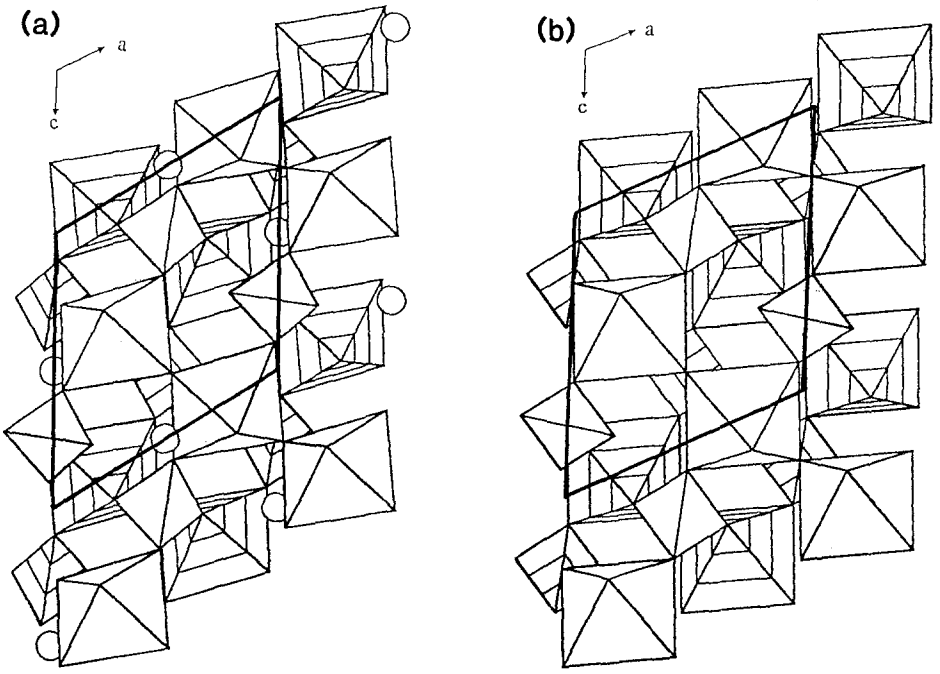

FIG. 4. [010] projections of the structure of (a) $Co_3(HPO_4)_2(OH)_2$. Circles represent the Co(2) atoms which occupy octahedra (not represented) sharing opposite faces with two neighboring Co(1) octahedra ($y \approx 1/4$: shaded; $y \approx 3/4$: unshaded). (b) $CoSO_4 \cdot H_2O$. The relation with $Co_3(HPO_4)_2(OH)_2$ is obvious.

At high temperature ($T > 120$ K), the susceptibility follows a Curie–Weiss law, $\chi = C/(T - \theta)$, with $C = 2.77$ per Co^{2+} and $\theta = -43$ K. When lowering the temperature a maximum appears at 18 K, then, after a broad minimum at around 15 K, a sharp peak is observed at 10.6 K.

At first sight, the χ^{-1} vs T curve down to

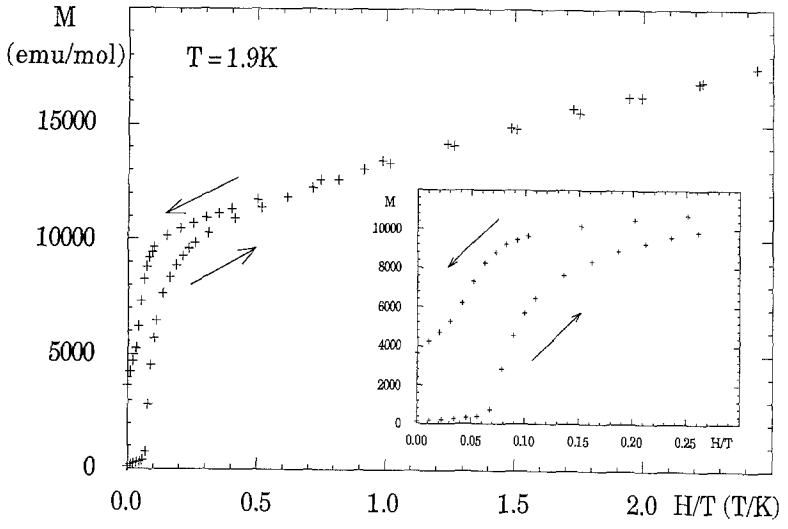

FIG. 5. Magnetization measurements at 1.9 K. The inset shows the low magnetic field portion.

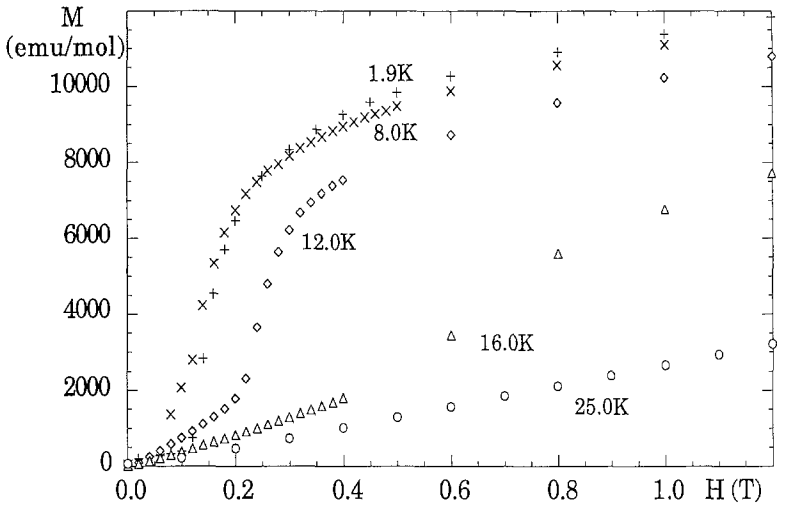

FIG. 6. Magnetization measurements at 1.9, 8, 12, 16, and 25 K.

18 K shows the main features of the behavior of a Co^{2+} cation in a distorted octahedral crystal field. Indeed, the degeneracy of the cubic $^4T_{1g}$ term is removed by the low symmetry, as well as by the spin–orbit coupling. Both effects produce six Kramers doublets and result in a doublet ground state (Fig. 10). Due to the value of the spin–orbit coupling constant ($-170\ cm^{-1}$ for the free ion) at low temperature ($T < 40$ K), the system may be described as having an *effective* spin $S = 1/2$. In this case the θ value obtained from the high temperature Curie–Weiss law comes from spin–orbit coupling instead of magnetic exchange interactions. The decrease in the χT vs T curve down to 35 K supports also this hypothesis.

Nevertheless, a careful examination of

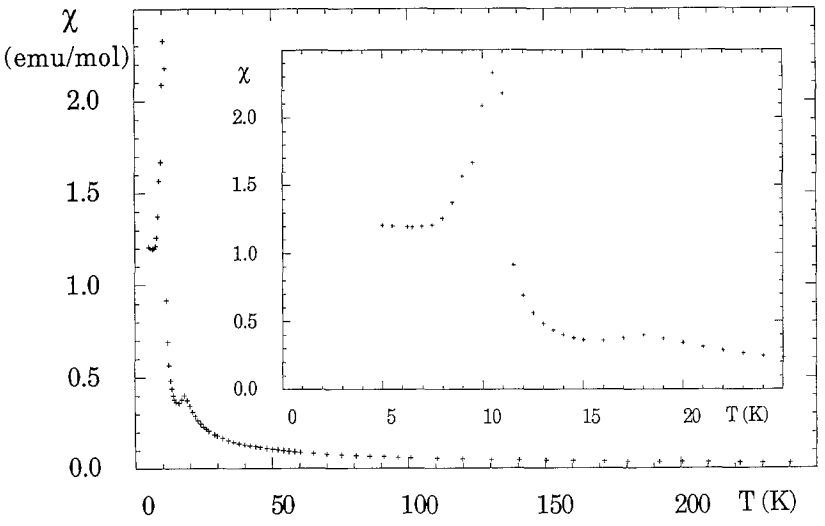

FIG. 7. Thermal evolution of χ in $Co_3(HPO_4)_2(OH)_2$ at $H = 0.1$ T.

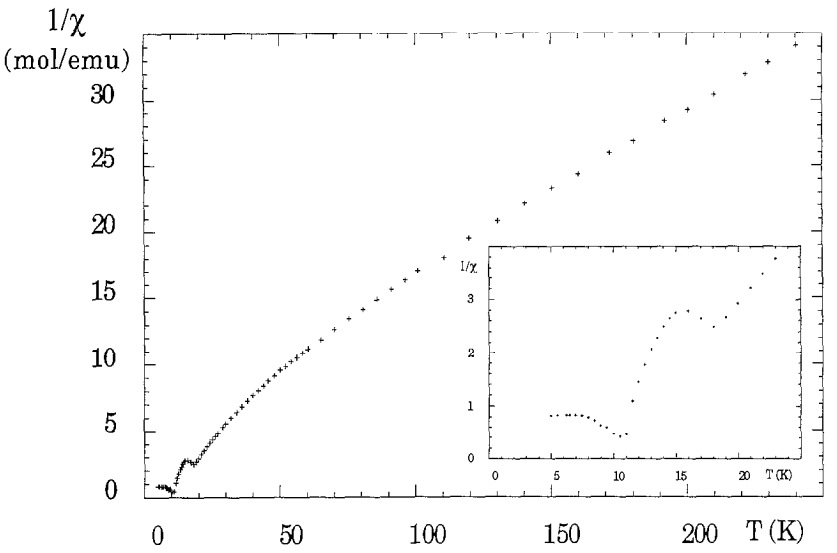

FIG. 8. Thermal evolution of χ^{-1} in $Co_3(HPO_4)_2(OH)_2$ at $H = 0.1$ T.

the curves of Figs. 7–9 shows that magnetic coupling must be taken into account. The increase of the χT vs T curve between 35 and 18 K can be viewed as the consequence of ferromagnetic interactions. Further increase of χT down to 11 K corresponds to the influence of another type of ferromagnetic coupling. An antiferromagnetic interaction leads to the $3D$ ordering observed at 10.6 K.

Discussion

The complex magnetic behavior of $Co_3(HPO_4)_2(OH)_2$ can be tentatively interpreted by considering the possible magnetic

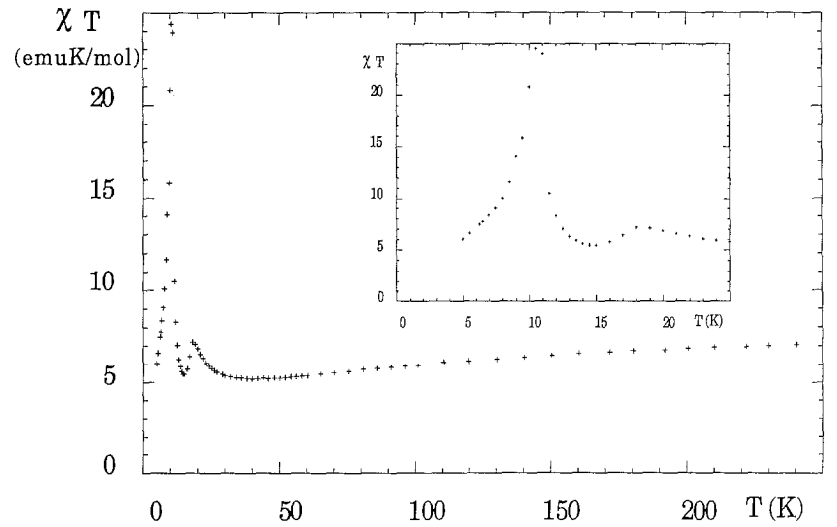

FIG. 9. Thermal evolution of χT in $Co_3(HPO_4)_2(OH)_2$ at $H = 0.1$ T.

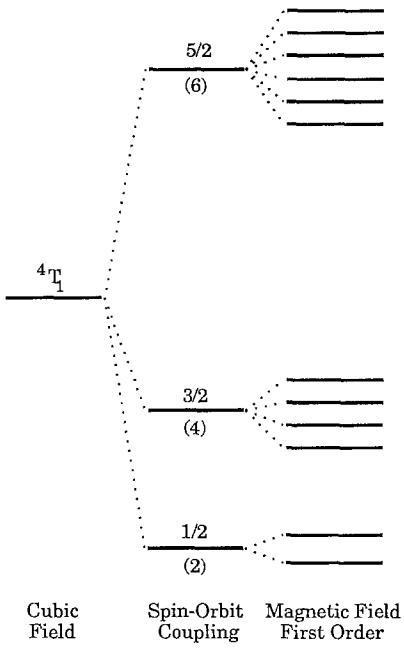

FIG. 10. Energy levels scheme for an isolated Co^{2+} ion in a distorted octahedral field.

interactions within the crystal structure. It has been described as formed by parallel layers linked by (HPO_4) tetrahedra and hydrogen bonds. A schematic view of a layer is given in Fig. 11. It appears that two types of interactions are predominant within such a layer:

(*i*) *Intratrimer interactions Co(1)–Co(2) through the common faces of the octahedra.* The direct interaction, which is antiferromagnetic, is weak because of the poor overlapping of the concerned magnetic orbitals, but other exchange interactions via O(2), O(4), and O(5) are expected to be strongly ferromagnetic as a result of the values of the angles Co(1)–O–Co(2), which are close to 90° ($Co(1)–O–Co(2)_{ave}$ = 85.7°). The involved mechanisms are of e_g–p_σ–p_σ'–e_g and t_{2g}–p_π–p_π'–t_{2g} type according to the Anderson–Goodenough–Kanamori rules (*30–32*).

(*ii*) *Intertrimer couplings Co(1)–Co(1) and Co(1)–Co(2) by a superexchange mechanism via O(5).* Considering the value of the Co–O–Co angle (averages 128.4° and 120.1(4)°, respectively), a rather complex either ferro- or antiferromagnetic coupling may occur.

The adjacent layers are coupled via the phosphate and the hydrogen bonds, giving rise to a 3*D* antiferromagnetic ordering at 10.6 K. Due to the complexity of the interactions as well as the strong anisotropy of the Co^{2+} ion, the magnetic moments are expected to be somewhat canted. Hence the metamagnetic transition at H_c = 0.12 T could correspond to the parallel alignment of the intralayer ferromagnetic components. A linear extrapolation for fields between 2.5 and 5 T allows the derivation of a net moment of ca. 11,000 emu/mole (0.65 BM per cobalt ion).

A further evidence of the ferromagnetic component within each layer is given by the thermal evolution of the remanent magnetization (Fig. 12): it begins to decrease and seems to vanish at a temperature close to T_N, but just above T_N a sudden increase is observed followed by a sharp peak. This

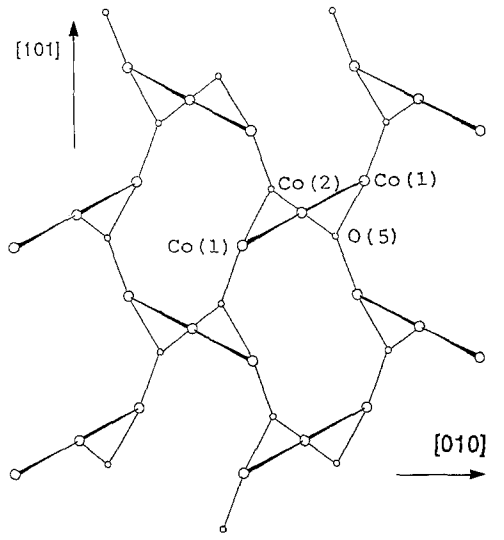

FIG. 11. Schematic view of a layer showing the intertrimer superexchange.

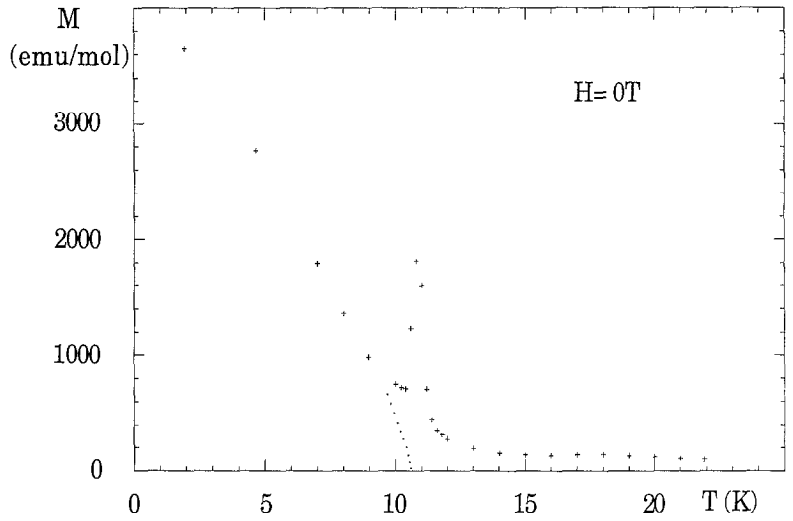

FIG. 12. Thermal evolution of the remanent magnetization. The dotted line corresponds to the normal evolution in a weak ferromagnet with $T = 10.6$ K.

rather surprising behavior may be ascribed to the intralayer ferromagnetic component masked at low temperature by the interplane antiferromagnetic coupling.

Neutron diffraction analysis is in progress in order to elucidate more clearly this complex magnetic structure as well as its thermal evolution up to 20 K.

Acknowledgments

J.L.P. thanks the Basque Government/Eusko Jaurlaritza for a doctoral Fellowship. The authors are greatly indebted to S. Martegoute for his technical assistance for the hydrothermal synthesis, and to J. Pannetier for his support in performing the neutron experiments at ILL.

References

1. E. MATTIEVICH AND J. DANON, *J. Inorg. Nucl. Chem.* **39,** 569 (1977).
2. H. C. MEIJER, J. VAN DEN HANDEL, AND E. FRIKKEE, *Physica* **34,** 475 (1967).
3. H. C. MEIJER, J. J. GIESEN, AND J. VAN DEN HANDEL, *Physica* **38,** 227 (1968).
4. H. C. MEIJER, T. W. ADAIR III, AND J. VAN DEN HANDEL, *Physica* **38,** 233 (1968).
5. S. C. ABRAHAMS, *J. Chem. Phys.* **44,** 2230 (1966).
6. V. FORSTAT, N. D. LOVE, J. N. MCELEARNEY, AND G. J. BUTTERWORTH, *Phys. Rev.* **1,** 3097 (1970).
7. J. B. FORSYTH, C. E. JOHNSON, AND C. WILKINSON, *J. Phys. C.* **3,** 1127 (1970).
8. J. L. PIZARRO, G. VILLENEUVE, AND L. M. LEZAMA, *Terra Abstracts* **1,** 293 (1989).
9. P. B. MOORE, "Mineral Assoc. Can. Handbook," Vol. 8, p. 267, Mineral Association of Canada (1982).
10. N. L. LINDBERG AND C. L. CHRIST, *Acta Crystallogr.* **12,** 695 (1959).
11. H. MORI AND I. ITO, *Acta Crystallogr* **3,** 1 (1950).
12. P. FEJDI, J. F. POULLEN, AND M. GASPERIN, *Bull. Mineral.* **103,** 135 (1980).
13. M. BLANCO, *Bol. Soc. Esp. Mineral.* **10**(2), 199 (1987).
14. P. E. WERNER, L. ERIKSSON, AND M. J. WESTDAHL, *J. Applied Crystallogr.* **18,** 367 (1985).
15. P. M. DE WOLFF, *J. Applied Crystallogr.* **1,** 108 (1968).
16. G. S. SMITH AND R. L. SNYDER, *J. Applied Crystallogr.* **12,** 60 (1979).
17. A. LE BAIL, H. DUROY, AND J. L. FOURQUET, *Mater. Res. Bull.* **23,** 447 (1988).
18. H. M. RIETVELD, *J. Applied Crystallogr.* **22,** 151 (1967).
19. H. M. RIETVELD, *J. Applied Crystallogr.* **2,** 65 (1969).
20. G. H. SHELDRICK, "SHELX 76, Program for Crystal Structure Determination," Univ. of Cambridge, London (1976).
21. "International Tables for X-Ray Crystallography," Vol. IV, Kynoch Press, Birmingham (1974).

22. T. SUZUKI, *Acta Crystallogr.* **13,** 279 (1960).
23. G. GIUSEPPETTI AND C. TADINI, *N. Jb. Miner. Mh.,* **9,** 410 (1983).
24. I.D. BROWN, "Structure and Bonding in Crystals," Vol. II, 1981, (M. O'Keeffe and A. Navrotsky, Eds.) p. 1, Academic Press.
25. D. B. WILES, A. SAKTHIVEL, AND R. A. YOUNG, Program DBW3.2S (1987).
26. D. B. WILES AND R. A. YOUNG, *J. Applied Crystallogr.* **14,** 149 (1981).
27. J. COING-BOYANT AND G. BASSI, *Compt. Rend. Acad. Sci. Paris* **256,** 1482 (1963).
28. J. M. BREGEAULT, P. HERPIN, J. M. MANOLI, AND G. PANNETIER, *Bull. Soc. Chim. Fr.* 4243 (1970).
29. P. LIGHTFOOT, A. K. CHEETHAM, AND A. W. SLEIGHT, *Inorg. Chem.* **26,** 3544 (1987).
30. P. W. ANDERSON, *Phys. Rev.* **13,** 1492 (1958).
31. J. B. GOODENOUGH, "Magnetism and the Chemical Bound," International Publ., New York (1963).
32. J. KANAMORI, *Phys. Chem. Solids* **10,** 87 (1959).